Binary dusty plasma Coulomb balls

S. W. S. Apolinario*
Departamento de Física, Universidade Federal de Pernambuco, 50670-901 Recife, PE, Brazil

F. M. Peeters†
Departement Fysica, Universiteit Antwerpen, Groenenborgerlaan 171, B-2020 Antwerpen, Belgium and Departamento de Física, Universidade Federal do Ceará, Caixa Postal 6030, Campus do Pia, 60455-760 Fortalesa, Ceará, Brasil

(Received 7 February 2011; published 29 April 2011)

We investigated the mixing and segregation of a system consisting of two different species of particles, having different charges, interacting through a pure Coulomb potential, and confined in a three-dimensional parabolic trap. The structure of the cluster and its normal mode spectrum are analyzed as a function of the relative charge and the relative number of different types of particles. We found that (a) the system can be in a mixed or segregated state depending on the relative charge ratio parameter and (b) the segregation process is mediated by a first or second order structural phase transition which strongly influences the magic cluster properties of the system.

DOI: 10.1103/PhysRevE.83.041136 PACS number(s): 64.60.−i

I. INTRODUCTION

In recent years, clusters of charged particles confined in traps have attracted considerable attention due to their successful applicability as a physical model to different important systems. As examples of such systems, we can site electrons in quantum dots [1] or on the surface of liquid helium [2], vortices in superfluids [3], ion traps [4], confined ferromagnetic particles [5], colloidal particles in circular traps [6], and charged dust particles in plasma traps [7]. Such finite size charged clusters also resemble Thomsoń "plum-pudding" model for the atom [8].

Only recently, the first experimental realization of a spherical three-dimensional cloud of monodisperse dust particles was realized [9]. Such an experiment was able to overcome the gravitational forces which usually lead the dust particles to form a quasi-two-dimensional (2D) structure. To realize a three-dimensional (3D) configuration a thermophoretic force was applied to compensate for gravity in combination with the plasma-induced electric field and a lateral external potential which results in a parabolic confinement. Such systems were named "Coulomb balls." Theoretical investigation of structural properties and melting behavior in 3D Coulomb balls are reported in Refs. [10–15].

Experimental realization of 3D isotropically confined binary systems must be possible both in ion traps and dusty plasma experiments. In the latter case, the most appropriated interparticle interaction potential to be considered would be the Yukawa potential. However, we would expect that in various limits our results would be valid to the case of a 3D binary Yukawa system.

Charged particles forming *large* 3D isotropic clusters arrange themselves in two different forms [14]. The center of the cloud is characterized by a body-centered cubic lattice, while particles close to the border form concentric spherical shells, and on the shell's surface particles create a hexagonal lattice with few dislocations and disclinations.

On the other hand, *small* 3D systems are formed by concentric and equally spaced shells carrying a specific number of particles. The number of shells depends on the total number of particles and in general, the number of shells increases with the number of particles. The ground state configuration of systems up to 12 particles consists of a single shell. These configurations in fact form three-dimensional regular polygons. From $N = 13$ up to 60 the arrangement of particles in the ground state (GS) configuration form two shells except for the clusters with $N = 58$ and 59 particles. For systems larger than 60 particles, ground state configurations start to appear with three shells [15].

Moreover, among the possible GS configurations there are few "magic" clusters whose shells obey an icosahedral or octahedral symmetry [15]. The latter alters the mechanical stability of the clusters, which leads to an enhanced value of the intrashell melting temperature. For a review about the dynamical and structural properties of 3D small clusters see Refs. [11,13,15,16].

The statical and dynamical properties of 2D systems consisting of two species' particles is well understood. For example, it was found in Refs. [17,18] that the charge ratio can function as an extra mechanism to adjust the value of the inter-ring melting temperature [19]. This results from the possibility of bringing together (apart) the internal and external rings of a 2D cluster and consequently increase (decrease) the commensurability between distinct rings. As a result, they observed variations in the melting temperatures of the binary clusters, with increased melting thresholds for intershell rotation and intershell particles when the symmetry of the inner cluster and the outer ring are commensurate. The latter was also found in Ref. [17] from a normal mode analysis.

In the present paper, we expand previous investigations [17,18] by considering small size systems consisting of particles of two different species, having different charges which are confined by an isotropic 3D potential. Because of the higher dimensionality of the 3D system, different physics are expected as compared to the 2D, 1D, and 0D counterparts. We considered N_A and N_B number of particles of species A and B which have a Q_A and Q_B charge, respectively. The physical properties of the system are determined by the

*sergio.apolinario@df.ufpe.br
†francois.peeters@ua.ac.be

parameters $\beta = Q_B/Q_A$ and $\chi = N_B/N$ with $N = N_A + N_B$ the total number of particles. Out of a few studies devoted to 3D systems of different-species particles, we would like to make note of two works: (1) Ref. [20] which considered a system with $N = 190$ particles and verified the existence of phase segregation induced by the size particles differences and (2) Ref. [21] which has shown for systems with unscreened Coulomb interactions containing 20 288 and 100 000 particles that the mixture of different components presents a stable configuration only if the particles of different species have the same mass-to-charge ratio. In contrast to the latter references, we devoted, in this paper, special attention to the investigation of structural phase transitions happening in small size systems, i.e., systems up to 38 particles.

We found that the two particles' species segregate into distinct shells. Moreover, we show in detail how magic cluster properties depend on the ratio of the number of distinct kinds of particles and the total number of shells in the cluster. We try to determine if a 3D binary system is able to exhibit intershell commensurability such as its 2D counterpart.

This paper is organized as follows. In Sec. II, the physical model and the numerical approaches are presented. In Secs. III A and III B we present our results for systems with small and large values of χ, respectively. This latter investigation is generalized to any value of χ in Sec. IV, while Sec. V considers the properties of magic clusters for systems with two shells. Finally, in Sec. VI we present our conclusions.

II. THEORETICAL MODEL

We study a 3D model system of N charged particles in an isotropic confinement potential, interacting through a repulsive Coulomb potential. We consider two species of particles A and B having a charge Q_A and Q_B, respectively. The potential energy of the system is given by

$$E = \sum_{i=1}^{N} \frac{1}{2} m\omega_0^2 \left(x_i^2 + y_i^2 + z_i^2\right) + \sum_{i>j=1}^{N_A} \frac{Q_A^2}{\epsilon_0} \frac{1}{|\mathbf{r}_i - \mathbf{r}_j|} + \sum_{k>l=1}^{N_B} \frac{Q_B^2}{\epsilon_0} \frac{1}{|\mathbf{r}_i - \mathbf{r}_j|} + \sum_{m=1}^{N_A} \sum_{n=1}^{N_B} \frac{Q_A Q_B}{\epsilon_0} \frac{1}{|\mathbf{r}_m - \mathbf{r}_n|}, \tag{1}$$

where ϵ_0 and m are, respectively, the dielectric constant and the particle mass, $\mathbf{r}_i = (x_i, y_i, z_i)$ is the coordinate of the ith particle, and N_A and N_B are the total number of particles, respectively, for the systems of type A and B. $N = N_A + N_B$ is the total number of particles and ω_0 is the confinement frequency. We rewrite the potential energy (2) in dimensionless form

$$E = \sum_{i=1}^{N} \left(x_i^2 + y_i^2 + z_i^2\right) + \sum_{i>j=1}^{N_A} \frac{1}{|\mathbf{r}_i - \mathbf{r}_j|} + \sum_{k>l=1}^{N_B} \frac{\beta^2}{|\mathbf{r}_i - \mathbf{r}_j|} + \sum_{m=1}^{N_A} \sum_{n=1}^{N_B} \frac{\beta}{|\mathbf{r}_m - \mathbf{r}_n|}, \tag{2}$$

where we defined the ratio of charges $\beta = Q_B/Q_A$ and express the coordinate and energy, respectively, in the following units: $r_0 = (2Q_A^2/m\epsilon_0\omega_0)^{1/3}$ and $E_0 = (m\omega_0^2 Q_A^4/2\epsilon_0^2)^{1/3}$. All our numerical results will be given in these units.

To obtain the stable configurations we used the Monte Carlo simulation technique supplemented with the Newton method in order to speed up the computation and to increase the accuracy of the found energy value (see Ref. [19] for details). By starting from a large number of different random initial configurations we are confident that we found the ground state configuration as long as the number of particles N is not too large, i.e., roughly $N < 60$. Depending on the total number of particles, between several hundred to several thousand random initial configurations were generated. The linear dynamics of the cluster was studied by investigating its normal modes.

The eigenfrequencies are the square root of the eigenvalues of the dynamical matrix

$$H_{\alpha\beta,ij} = \left. \frac{\partial^2 V}{\partial r_{\alpha,i} \partial r_{\beta,j}} \right|_{r_{\alpha,i} = r^n_{\alpha,i}}, \tag{3}$$

where $\{r^n_{\alpha,i}; \alpha = x,y,z; i = 1,...,N\}$ are the positions of the particles in a stable configuration.

III. ONE SHELL SYSTEM

Small isotropically confined systems of charged classical particles are interesting toy models that exhibit a rich variety of properties related to finite size effects. In this section we investigate the effect of the charge ratio $\beta = Q_B/Q_A$ and the ratio between the different number of particles $\chi = N_B/N$ on the GS and the eigenfrequencies of a few representative small systems.

In order to avoid a complicated analysis but still acquire satisfactory knowledge of mechanical processes induced by the charge ratio parameter we first investigate relatively small systems with only $N = 12$ particles. It has already been known for some time [22] that the GS configuration of a monodisperse ($\beta = 1$) system with $N = 12$ particles forms a magic cluster. Magic clusters with one shell have an enhanced mechanical stability which is reflected in a large value of the lowest nonzero eigenfrequency and large melting temperatures [13,15,19].

A. Small value of χ

We start by investigating the influence of the charge ratio parameter β by considering systems with a relatively small number of particles of the B specie. Figure 1(a) shows the eigenfrequency spectrum for the system with $N = 12$ particles and $\chi = 0.167$ (i.e., $N_A = 10$ and $N_B = 2$) as functions of the charge ratio. Notice that for $\beta = Q_B/Q_A = 1$ the normal modes are highly degenerate which is typical for symmetric configurations, i.e., magic clusters. We can see that of the total of 36 normal modes present in any 3D system with $N = 12$ confined particles, there are only ten different values for the eigenfrequencies. However, even a small decrease of the charge ratio β disturbs the symmetry of the cluster and the degeneracies in the frequencies are lifted [see Fig. 1(a)]. This fact indicates that properties of magic clusters are strongly sensitive to the charge ratio.

When further decreasing β, one notices that at the critical value $\beta_c = 0.879$ there is an abrupt discontinuity of the eigenfrequencies [see the black downward arrow in Fig. 1(a)], which corresponds to a structural phase transition [23]. In

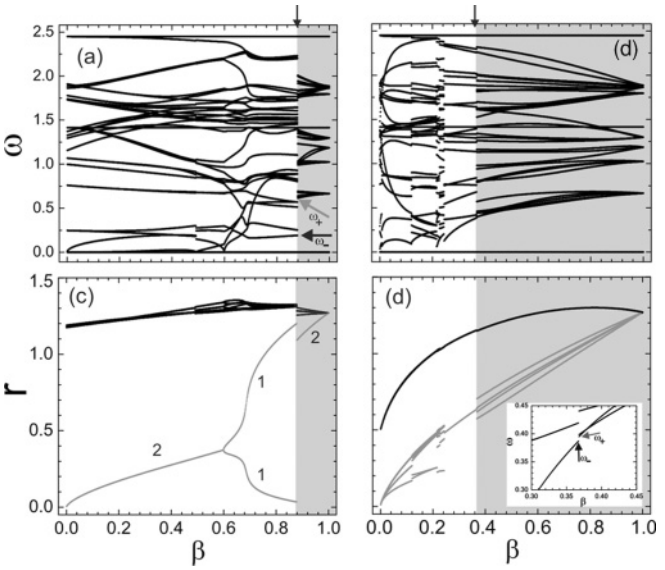

FIG. 1. The eigenfrequency spectrum (a) and the radial position (c) of the different particles as functions of the charge ratio β for the system with $N = 12$ and $\chi = 0.167$ (i.e., $N_A = 10$ and $N_B = 2$). (b) and (d) are the same but for the system with $N = 12$ and $\chi = 0.833$ (i.e., $N_A = 2$ and $N_B = 10$). The inset in (d) shows in detail the eigenfrequencies' dependence ω for values of the charge ratio parameter close to the critical value $\beta_c = 0.380$. The numbers in (c) indicate how many particles have the same radius. In (c) and (d) the black and gray curves present, respectively, the radius of particles of types A and B.

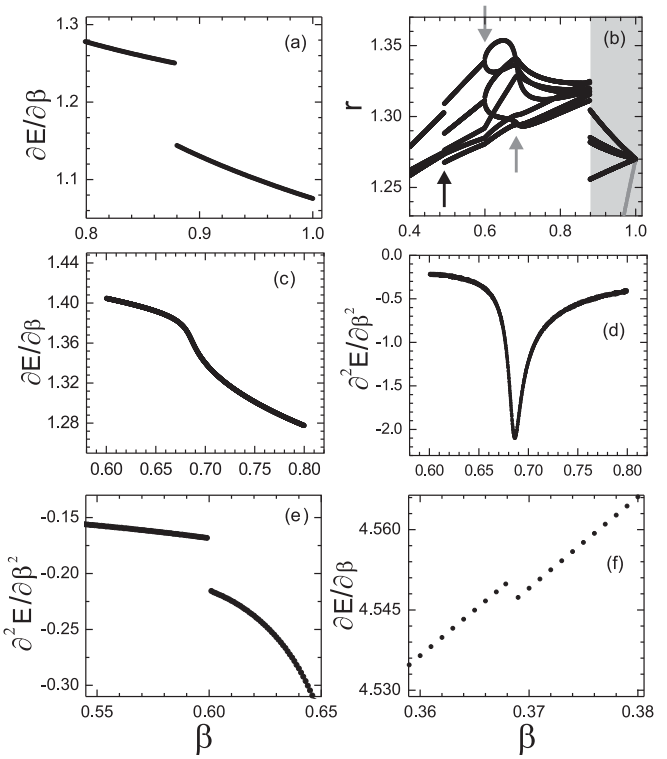

FIG. 2. For the system with $N = 12$ particles and $\chi = 0.167$, (a) and (c) [(d) and (e)] display the first (second) derivatives of the energy E with respect to β while (b) shows a zoom of Fig. 1(c). (f) displays the first derivative of the energy E with respect to the charge ratio parameter β for the system with $N = 12$ particles and $\chi = 0.833$.

order to reveal the nature of this transition, we calculated the first derivative of the energy E with respect to the charge ratio β. The latter is shown in Fig. 2(a). The first derivative is discontinuous at the critical point $\beta_c = 0.879$ which shows that we have a first order structural phase transition.

The distribution of particles along the radial direction is strongly sensitive to the charge ratio parameter around this first order structural phase transition as we can see in Fig. 1(c). The latter figure displays the distance r of the particles from the center, as a function of β. Initially, for a decreasing value of β, the one shell configuration gradually forms a set of five subshells. The two B particles, which have the same radius, move toward the center [gray curve in Fig. 1(c)]. The latter is shown in some detail in Fig. 2(b), i.e., the four subshells formed by particles of the A type [four black curves within the gray region in Fig. 2(b)] and the two particles of the B type having the same radius [gray curve in Fig. 2(b)]. Eventually, when the charge ratio parameter achieves the critical value $\beta_c = 0.879$, one of the B particles jumps to the center.

Most importantly, for decreasing values of the charge ratio parameter, the first nonzero eigenfrequency decreased abruptly at the critical point $\beta_c = 0.879$, i.e., from $\omega_+ = 0.61$ to $\omega_- = 0.19$, which are indicated, respectively, by the gray and black arrows in Fig. 1(a). We use the subscripts $(+)$ and $(-)$ in ω to indicate the first nonzero eigenfrequency at a value of β slightly larger and smaller than the critical charge ratio parameter β_c. From the latter fact we can conclude that for $\beta > \beta_c = 0.879$ [gray region in Figs. 1(a) and 1(c)] the system still exhibits magic cluster properties, while for $\beta < \beta_c = 0.879$ these properties are completely lost.

Additionally, note also that the radius of the particles belonging to the subshells of the system with $N = 12$ and $\chi = 0.167$ also passes though a plastic deformation at the value $\beta_c = 0.686$ [see the upward gray arrow in Fig. 2(b) which is a zoom of Fig. 1(c)]. As we can see from Figs. 2(c) and 2(d), i.e., the first and second derivatives of the energy with respect to the charge ratio parameter β, respectively, there is no discontinuity for values of the charge ratio parameter close to the critical point $\beta_c = 0.686$. However, we can see clearly from Fig. 2(d) that the third derivative of the energy with respect to the charge ratio parameter will be discontinuous at the critical point $\beta_c = 0.686$ (minimum of the curve) which indicates a structural phase transition of the third order.

Figure 3 shows plots of the clusters' configuration for a few different values of β, where black and red (gray) balls indicate, respectively, particles of type A and B, and bonds between particles of the same type are drawn only to enhance visualization. The clusters for $\beta = 0.9$ and 0.8, i.e., before and after the first order structural phase transition that occurs at $\beta_c = 0.879$, are shown, respectively, in Figs. 3(c) and 3(b). Notice that the GS configuration of Fig. 3(c) is still formed by one single (quasi-) shell, while after the transition, one particle moves to the center of the cluster, as shown in Fig. 3(b).

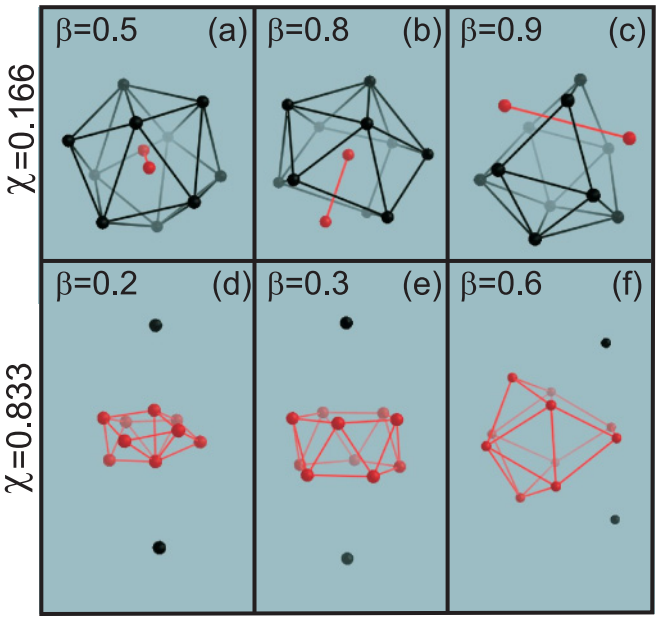

FIG. 3. (Color online) Ground state configurations for the system with $N = 12$, $\chi = 0.166$ (first row), $\chi = 0.833$ (second row) and different values of the charge ratio parameter β as indicated in figures. The black and red (gray) balls represent, respectively, particles of the type A and B and bonds between balls are only to enhance visualization.

The system undergoes a second structural phase transition at $\beta_c = 0.491$. The latter transition corresponds to a reorganization of particles belonging to the external shell [see the black upward arrow in Fig. 2(b)] where the number of subshells in the external shell decreases discontinuously from 5 to 3. The first derivative of the energy as a function of β is not presented here but it is discontinuous at the critical value $\beta_c = 0.491$.

Three-dimensional finite systems of binary charged particles also undergo structural phase transitions of the second order. For the latter case, the first derivative of the energy with respect to the charge ratio remains continuous while its second derivative exhibits a discontinuity. Such a transition can be seen, for example, at the critical value $\beta_c = 0.6$, as demonstrated by the second derivative of the energy with respect to β in Fig. 2(e). This is a continuous transition mediated by the softening of a normal mode, i.e., one of the eigenfrequencies decreases to zero as shown in Fig. 1(a).

Note that this second order structural phase transition at $\beta_c = 0.6$ results in an enhancement of the structural order of the whole cluster, since (1) the two internal particles move toward a position with the same distance $r = 0.32$ from the center of the cluster as shown in Fig. 1(c) and (2) the number of subshells belonging to the external shell is reduced from 7 to 5 [see the gray downward arrow in Fig. 2(b)].

Figure 3(a) shows the cluster configuration of the GS for $\beta = 0.5$, i.e., just after the second order structural phase transition that occurs at $\beta_c = 0.6$. Note that the two less charged particles [red (gray) balls] are located in the interior of the cluster and are topologically separated from the rest of the particles, therefore it becomes evident that decreasing β leads, as a final result, to a topological phase segregation between particles of different species A and B.

B. Large value of χ

In the previous section we demonstrated that for systems with a small value of the relative number of different types of particles, i.e., $\chi = 0.167$, as a function of β, structural phase transitions are found of first and second order. Furthermore, as the charge ratio parameter β decreases, the less charged particles (particles of specie B) segregates from the more charged particles (particles of specie A). Such a phenomenon of particle segregation was found to modify the magic cluster properties of the system, which became evident by the large drop of the first nonzero eigenfrequency that was mediated by a structural phase transition of the first order. In this section, we investigated if the latter physical phenomena are also present in a system with a large χ value.

Figure 1(b) shows the eigenfrequencies for the system with $N = 12$ particles and $\chi = 0.833$, i.e., $N_A = 2$ and $N_B = 10$, as a function of the charge ratio parameter β. Note that the system undergoes a first order structural phase transition at $\beta_c = 0.38$, which is indicated by a discontinuity in both: the eigenfrequencies [see the black downward arrow in Fig. 1(b)] and the first derivative of the energy with respect to the charge ratio parameter β as shown in Fig. 2(f).

Note that for $\beta > \beta_c = 0.380$ [gray region in Fig. 1(b)], the cluster exhibits an arrangement which is reminiscent for an icosahedral structure [see Fig. 3(f) for], and no structural phase transition is seen in this β region. Moreover, along this gray region the first nonzero eigenfrequency decreases gradually from $\omega = 0.66$ to 0.39, when the charge ratio parameter decreases from $\beta = 1.00$ to 0.38. The latter fact shows that for $\chi = 0.833$ the system undergoes a continuous crossover where the properties of magic cluster are reduced gradually as the value of β is decreased.

When further decreasing β the GS configuration becomes a highly symmetric structure [see Fig. 3(e) for $\beta = 0.30$] where the positions of all particles of the B type converge to the same radius $r = 0.52$ as shown in Fig. 1(d). This configuration has a similar symmetry as the one found in magic clusters of monodisperse anisotropically confined particles [24,25], i.e., the so-called multiple ring structures. In the latter case, the cluster exhibits distinct properties, such as a large value of the critical melting temperature and a large lowest energy eigenfrequency.

Ultimately, note that for lower values of the charge ratio parameter, i.e., for $\beta = 0.1$–0.4, the system passes through a sequence of first order structural phase transitions which occur at $\beta = 0.37, 0.24, 0.23, 0.21$, and 0.12. The latter fact strongly suggests that for a small value of β there will be a substantial decrease of the melting temperature of the system [13,25]. A typical configuration found within this latter region is shown in Fig. 3(d) for $\beta = 0.20$.

C. Intermediate values of χ

From the latter two sections we found that the transition *magic-to-normal cluster* can occur via two distinct paths: through an abrupt (first order) or a gradually (crossover) transition for systems with extreme values of χ, i.e., $\chi = 0.167$ and 0.876. In order to obtain general trends about the magic-to-normal cluster transition, we extend in this section

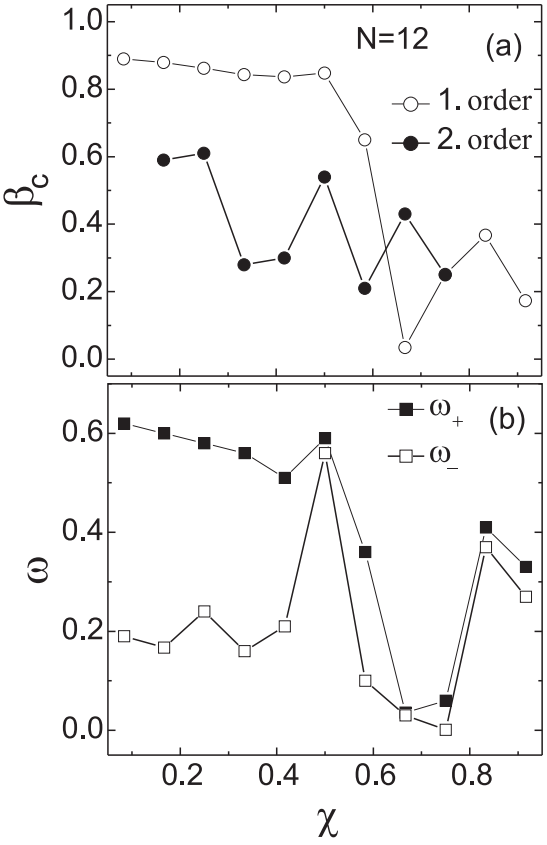

FIG. 4. Critical charge ratio parameter β_c related to a first (opened circle) and a second (closed circle) order structural phase transition and (b) the lowest energy eigenfrequencies ω_+ and ω_- computed, respectively, for a value of β slightly larger and smaller than the critical charge ratio β_c. Both quantities are plotted as a function of the relative number of different types of particles.

our previous investigation by considering the magic cluster with $N = 12$ particles for several values of χ.

Figure 4(a) plots the critical charge ratio parameter β_c related to first (opened circles) and second (closed circles) order structural phase transitions as a function of χ for the one shell system with $N = 12$ particles. From Fig. 4(a) we notice that for $\chi \leqslant 0.5$ the value of the critical charge ratio parameter is relatively large, i.e., $\beta_c \simeq 0.9$, while it drops to a value smaller than $\beta_c = 0.3$ for $\chi \geqslant 0.65$. Additionally, notice that as the charge ratio parameter β is decreased from 1.0 to 0.0 for systems with $\chi \leqslant 0.60$ ($\chi > 0.60$), the first structural phase transition is of first (second) order.

Figure 4(b) displays, as a function of χ, the eigenfrequencies ω_+ and ω_- obtained for values of the charge ratio parameter, respectively, slightly larger and smaller than β_c. Note that for the range $0.0 \leqslant \chi \leqslant 0.4$ we have $\omega_+ > 0.5$ which indicates that for this interval of χ and for $\beta < \beta_c$ the system exhibits magic cluster properties. The magic cluster properties are lost for values of β smaller than the critical charge ratio parameter as indicated by the small values of the eigenfrequencies just after the transition, i.e., $\omega_- < 0.40$ for $\chi \leqslant 0.45$. From the latter facts we can conclude that for small values of χ, i.e., for $\chi \leqslant 0.45$, the transition magic-to-normal cluster is well defined and mediated by a structural phase

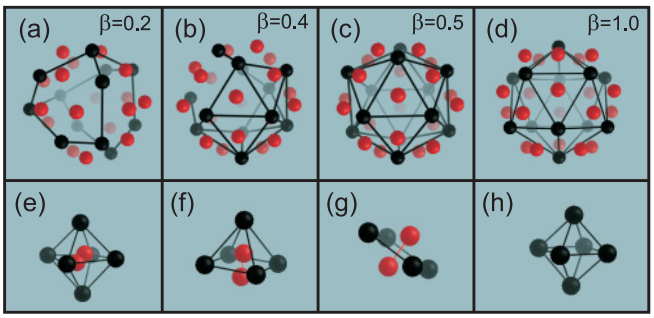

FIG. 5. (Color online) Particles' arrangement of the external shell (first line) and the internal shell (second line) of the GS configuration of the system with $N = 38$ particles; $\chi_1 = 0.33$ and $\chi_2 = 0.0$. Configurations in the same column have the same critical charge ratio parameter β which are given in the figures. In the top panels all particles are of the same type, and red (gray) and black balls represent, respectively, five- and sixfold particles. On the second line, particles of the A and Btypes are represented, respectively, by black and red (gray) balls. Bars between the different balls are used to enhance visualization.

transition of the first order. Note that we cannot conclude the same for systems with larger values of χ, since for $\chi > 0.5$ the value of ω_+ is already small, i.e., $\omega_+ < 0.4$. The latter facts demonstrate that for a system with one shell and large values of χ the magic-to-normal cluster transition evolves gradually as β decreases, i.e., without the mediation of a first order structural phase transition.

IV. TWO SHELL SYSTEMS

In this section we investigate, for large size systems, e.g., clusters with two shells, the mechanisms that are responsible for a particle's segregation and its dependencies on the parameter χ. We consider the system with $N = 38$ particles which is a magic cluster when $\beta = 1$.

The magic cluster structure of the system with $N = 38$ particles is formed by two concentric shells with arrangement (6,32), i.e., 6 and 32 particles forming, respectively, the internal and external shells [13,15]. Such a configuration, for the monodisperse case, is shown in Figs. 5(d) and 5(h), respectively, for the external and internal shells. Note that the external shell [see Fig. 5(d)] has two types of particles topologically distinct, i.e., five- and sixfold particles which are surrounded by, respectively, five and six neighboring particles. The five- and sixfold particles are represented by black and red (gray) balls in Fig. 5(d) and we have 20 fivefold and 12 sixfold particles, respectively. Note that the fivefold particles form an icosahedron, while each of the sixfold particles are symmetrically positioned near the sides' center of the polygon. Such an arrangement results in a closure of the external shell which is responsible for the large mechanical stability against intrashell melting [13].

A detailed analysis was realized in Ref. [13] in order to determine the normal mode related to the mechanical stability of the external shell. As a result it was shown that the fourth nonzero lowest energy eigenfrequency is related to the mechanical stability of the cluster, i.e., the larger the fourth nonzero lowest energy eigenfrequency, the more stable the

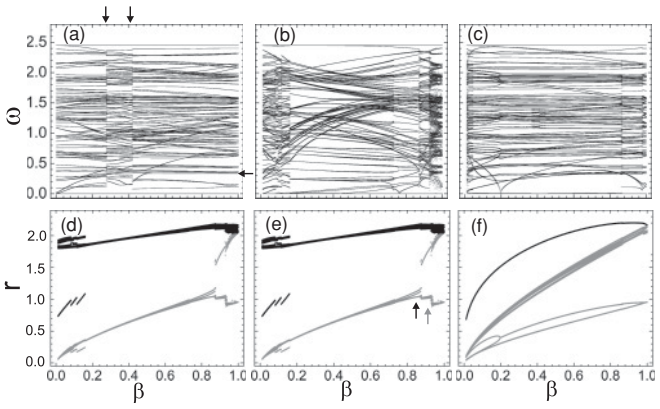

FIG. 6. The top and bottom panels show systems with $N = 38$ particles and, respectively, the eigenfrequencies and the radial positions of particles as a function of the charge ratio parameter β. Figures in the same column are related to the same system. From left to right, figures in the first, second, and third columns, correspond, respectively, to the parts of parameters $\chi_1 = 0.33$ and $\chi_2 = 0.0$, $\chi_1 = 1.0$ and $\chi_2 = 0.125$, and $\chi_1 = 1.0$ and $\chi_2 = 0.938$. In (d), (e), and (f) the black and gray curves represent, respectively, the radius of particles of types A and B.

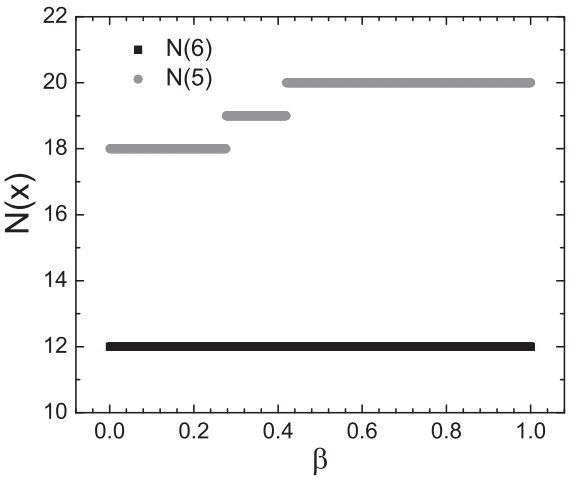

FIG. 7. The number of particles in the external shell, $N(x)$, having x nearest neighboring other particles in the same shell, as a function of the charge ratio parameter β for the system with $N = 38$ particles; $\chi_1 = 0.33$ and $\chi_2 = 0.0$.

external shell is. The eigenfrequency mode for a monodisperse system, i.e., a system with $\beta = 1.0$, is equal to $\omega = 0.43$. It has already known for some time that only the fourth nonzero lowest energy eigenfrequency is important for the analysis of the cluster stability [13].

For large systems we found that it is convenient to define the ratio of the different types of particles χ for each one of the shells. Accordingly, $\chi_i = N_B^{(i)}/N^{(i)}$, where $N_B^{(i)}$ and $N^{(i)}$ are, respectively, the number of particles of type B and the total number of particles in the ith shell, where "i" can stand for 1 and 2, respectively, for the internal and external shells.

Figure 6 displays the eigenfrequencies (top panel) and the radial position of each particle (bottom panels) against the charge ratio parameter β for systems with $N = 38$ particles and different values of χ_1 and χ_2. For the system with $N = 38$ particles, $\chi_1 = 0.33$ and $\chi_2 = 0.0$ [see Figs. 6(a) and 6(d)], a first order structural phase transition occurs at the two critical values $\beta_c = 0.419$ and 0.273 [see the black downward arrows in Fig. 6(a)]. Moreover, note that the fourth lowest nonzero eigenfrequency [see the leftward black arrow in Fig. 6(a)], for the interval $0.419 = \beta_c < \beta < 1.0$, has a large eigenfrequency value, i.e., $\omega \simeq 0.43$. Figure 7 displays the number of particles with five [$N(5)$, see the gray circles in Fig. 7] and six [$N(6)$, see the black squares in Fig. 7] first neighboring particles, i.e., the coordination number, computed on the external shell as a function of β. Notice that within the latter interval, i.e., $0.419 = \beta_c < \beta < 1.0$, the number of five- and sixfold particles remains, respectively, equal to 20 and 12. Therefore we can conclude that, within the interval $0.419 = \beta_c < \beta < 1.0$, the GS configuration still exhibits magic cluster properties [13,15]. Figures 5(c) and 5(g) display, respectively, the external and internal shells of the system with $N = 38$ particles with $\chi_1 = 0.33$, $\chi_2 = 0.0$, and $\beta = 0.5$. Accordingly, we can see that the external shells shown in Figs. 5(c) and 5(d) have the same symmetry. However, we cannot arrive at the same conclusion for the internal shell. The two particles of B type [(red) gray balls in Fig. 5(g)] and the four particles of A type [black balls in Fig. 5(g)] have radii equal to $r = 0.2$ and $r = 0.8$, respectively. Note that the latter configuration is different from the octahedral configuration found for $\beta = 1.0$, which is shown in Fig. 5(h). The latter facts demonstrate that, for the parameters chosen above, the internal shell is more sensitive to a decrease of the charge ratio parameter than the external one.

From Figs. 6(b) and 6(e) we notice that the system with $\chi_1 = 1.0$, $\chi_2 = 0.125$, and $N = 38$ passes through a large number of first order structural phase transitions for values of the charge ratio parameter close to one, i.e., roughly $\beta > 0.936$.

For values of the charge ratio parameter larger than $\beta = 0.936$ [indicated by the upward gray arrow in Fig. 6(e)] the internal shell still has six particles of B type. Between the values $\beta = 0.936$ [indicated by the upward gray arrow in Fig. 6(e)] and $\beta = 0.876$ [indicated by the upward black arrow in Fig. 6(e)], the internal shell has two extra particles of B type, i.e., it has eight particles in total. Finally, for $\beta < 0.876$ all ten particles of B type form the internal shell.

It becomes clear from Figs. 6(b) and 6(e) that the region of successive first order structural phase transitions is related to a mixed state where particles of A and B types coexist in the external shell. Such a mixed state presents a huge number of minimum energy configurations with energies very close to each other, and therefore, a slight variation of the charge ratio parameter results in a different GS configuration.

Despite this additional complication, i.e., the presence of a vitric phase for values of β close to one, we still can conclude that the migration of particles from the external shell toward the internal one happens for a large value of the charge ratio parameter, i.e., for $\beta \simeq 0.876$. The latter is in concordance to the fact that χ_2 is relatively small, i.e., $\chi_2 = 0.125$. However, a detailed analysis of the mechanical stability of the cluster based on the fourth nonzero lowest energy eigenfrequency and the number of first neighboring particles would be difficult due to the presence of the vitric phase. Nevertheless, from Figs. 6(b) and 6(e) we can clearly conclude that for $\beta < 0.85$ the external

shell does not exhibit the closure condition found in a magic cluster since it has only 31 particles.

Finally, Figs. 6(c) and 6(f) show, respectively, the eigenfrequencies and the radial position of particles for the system with $\chi_1 = 1.0$, $\chi_2 = 0.938$, and $N = 38$ particles. From the latter figures it is clear that there are no indications of structural phase transitions of the first order related to the migration of particles from the external shell towards the internal one. The latter is in concordance of the fact that the relative number of different types of particles on the external shell is relatively large, i.e., $\chi_2 = 0.938$.

V. CONCLUSION

We considered a 3D binary system of two distinct types of particles differing from each other by their charge, interacting through a repulsive Coulomb potential, and trapped together by an external isotropic confinement potential. The mechanical stability of magic clusters in 3D systems were investigated as a function of the clusters' parameters: the charge ratio β, the total number of particles N, and the parameter χ_i, which gives the relative number of particles of B type in the ith shell.

Our investigation of the magic cluster properties of 3D binary systems were focused on two representative systems: the system with $N = 12$ and 38 particles, where the GS configurations for $\beta = 1.0$ consist of one and two shells, respectively, and both form a magic cluster.

We have found that independently of the cluster size decreasing, the charge ratio parameter ultimately brings particles of B type towards the internal region of the cluster. As a result, a decrease of the charge ratio parameter causes the segregation of the different types of particles and leads the cluster to lose its magic cluster properties. Such a magic-to-normal cluster transition was found to be strongly dependent on the relative number of different types of particles per shell.

For the system with $N = 12$ particles, i.e., the system with one shell, and decreasing values of the charge ratio parameter β, the magic-to-normal cluster transition was found to evolve in two distinct ways depending on the magnitude of χ: (1) for small values of χ, i.e., $\chi \leqslant 0.6$, the magic-to-normal cluster transition occurred through a first order structural phase transition and (2) for large values of χ, i.e., $\chi \geqslant 0.7$, the magic-to-normal cluster transition evolved gradually without the mediation of a first order structural phase transition.

Therefore, for the system with one shell, a normal mode analysis was able to determine precisely, the region of the charge ratio parameter β within which the system exhibits magic cluster properties. We could not develop the same analysis for large systems with two shells due to the presence of a vitric phase. Nevertheless, the magic-to-normal cluster transition in large systems showed similar behavior to the one found in small systems, i.e., for small values of χ, the magic-to-normal cluster transition occurs through a first order structural phase transition, while for large values of χ, there is a continuous crossover.

For systems with small χ_i and a decreasing value of β, there are not enough particles of B type belonging to the ith shell to form by themselves an extra shell. Additionally, we know that close to the monodisperse regime ($\beta \simeq 1.0$), configurations having an isolated set of particles, i.e., those that do not form a shell, will tend to be less energetically favorable than configurations having all particles confined in a shell. The latter is the reason for the first order structural phase transition occurring for large values of β, i.e., for $\beta \simeq 1.0$, when the parameter χ is small.

Additionally, we found that binary systems can exhibit a particular configuration called multiple ring structure as shown in Fig. 3(e). This kind of configuration was found to exhibit magic cluster properties as shown in Ref. [25].

Finally, note that since the differences of energies between the ground state of nonmagic clusters and the metastable states are usually very small, metastable states can be easily accessible via a slight increase of temperature. Therefore, results involving structural phase transitions of the ground state configuration of nonmagic clusters are, in general, not valid for temperatures other than zero. However, note that such a picture is different for magic clusters since they hold large mechanical stability, which is responsible for keeping the symmetry of the cluster even for temperatures relatively large, i.e., for temperatures close to the melting temperature.

ACKNOWLEDGMENTS

This work was supported by FACEPE (Fundação de Amparo à Ciência e Tecnologia do Estado de Pernambuco) and the Flemish Science Foundation (FWO-Vl).

[1] M. A. Reed and W. P. Kirk, *Nanostructure Physics and Fabrication* (Academic Press, Boston, 1989).
[2] P. Leiderer, W. Ebner, and V. B. Shikin, Surf. Sci. **113**, 405 (1987).
[3] Y. Kondo, J. S. Korhonen, M. Krusius, V. V. Dmitriev, E. V. Thuneberg, and G. E. Volovik, Phys. Rev. Lett. **68**, 3331 (1992).
[4] B. G. Levi, Phys. Today **41**(2), 17 (1988).
[5] M. Golosovsky, Y. Saado, and D. Davidov, Phys. Rev. E **65**, 061405 (2002).
[6] R. Bubeck, C. Bechinger, S. Neser, and P. Leiderer, Phys. Rev. Lett. **82**, 3364 (1999).
[7] W.-T. Juan, Z.-H. Huang, J.-W. Hsu, Y.-J. Lai, and Lin I, Phys. Rev. E **58**, R6947 (1998).
[8] J. J. Thomson, Philos. Mag. **7**, 237 (1904).
[9] O. Arp, D. Block, A. Piel, and A. Melzer, Phys. Rev. Lett. **93**, 165004 (2004).
[10] M. Bonitz, D. Block, O. Arp, V. Golubnychiy, H. Baumgartner, P. Ludwig, A. Piel, and A. Filinov, Phys. Rev. Lett. **96**, 075001 (2006).
[11] P. Ludwig, S. Kosse, and M. Bonitz, Phys. Rev. E **71**, 046403 (2005).
[12] V. Golubnychiy, H. Baumgartner, M. Bonitz, A. Filinov, and H. Fehske, J. Phys. A **39**, 4527 (2006).
[13] S. W. S. Apolinario and F. M. Peeters, Phys. Rev. E **76**, 031107 (2007).
[14] R. W. Hasse and V. V. Avilov, Phys. Rev. A **44**, 4506 (1991).

[15] S. W. S. Apolinario, B. Partoens, and F. M. Peeters, New J. Phys. **9**, 283 (2007).
[16] M. Bonitz, C. Henning, and D. Block, Rep. Prog. Phys. **73**, 066501 (2010).
[17] W. P. Ferreira, F. F. Munarin, K. Nelissen, R. N. Costa Filho, F. M. Peeters, and G. A. Farias, Phys. Rev. E **72**, 021406 (2005).
[18] J. A. Drocco, C. J. Olson Reichhardt, C. Reichhardt, and B. Jankó, Phys. Rev. E **68**, 060401(R) (2003).
[19] V. A. Schweigert and F. M. Peeters, Phys. Rev. B **51**, 7700 (1995).
[20] S. G. Psakhie, K. P. Zolnikov, L. F. Skorentsev, D. S. Kryzhevich, and A. V. Abdrashitov, Phys. Plasmas **15**, 053701 (2008).
[21] T. Matthey, J. P. Hansen, and M. Drewsen, Phys. Rev. Lett. **91**, 165001 (2003).
[22] K. Tsuruta and S. Ichimaru, Phys. Rev. A **48**, 1339 (1993).
[23] B. Partoens, V. A. Schweigert, and F. M. Peeters, Phys. Rev. Lett. **79**, 3990 (1997).
[24] S. W. S. Apolinario, B. Partoens, and F. M. Peeters, Phys. Rev. B **77**, 035321 (2008).
[25] S. W. S. Apolinario and F. M. Peeters, Phys. Rev. B **78**, 024202 (2008).